Contents lists available at ScienceDirect

Colloids and Surfaces B: Biointerfaces

Peptide-laden mesoporous silica nanoparticles with promoted bioactivity and osteo-differentiation ability for bone tissue engineering

Zuyuan Luo [a,b,1], Yi Deng [a,b,1], Ranran Zhang [c], Mengke Wang [a], Yanjie Bai [d], Qiang Zhao [d], Yalin Lyu [c], Jie Wei [e], Shicheng Wei [a,b,*]

[a] *Department of Oral and Maxillofacial Surgery, School and Hospital of Stomatology, Peking University, Beijing 100081, China*
[b] *Center for Biomedical Materials and Tissue Engineering, Academy for Advanced Interdisciplinary Studies, Peking University, Beijing 100871, China*
[c] *Department of Stomatology, Beijing Anzhen Hospital, Capital Medical University, Beijing 100029, China*
[d] *Department of Stomatology, Aviation General Hospital of China Medical University and Beijing Institute of Translational Medicine, Chinese Academy of Science, Beijing 100012, China*
[e] *Key Laboratory for Ultrafine Materials of Ministry of Education, East China University of Science and Technology, Shanghai 200237, China*

ARTICLE INFO

ABSTRACT

Combination of mesoporous silica materials and bioactive factors is a promising niche-mimetic solution as a hybrid bone substitution for bone tissue engineering. In this work, we have synthesized biocompatible silica-based nanoparticles with abundant mesoporous structure, and incorporated bone-forming peptide (BFP) derived from bone morphogenetic protein-7 (BMP-7) into the mesoporous silica nanoparticles (MSNs) to obtain a slow-release system for osteogenic factor delivery. The chemical characterization demonstrates that the small osteogenic peptide is encapsulated in the mesoporous successfully, and the nitrogen adsorption–desorption isotherms suggest that the peptide encapsulation has no influence on mesoporous structure of MSNs. In the cell experiment, the peptide-laden MSNs (p-MSNs) show higher MG-63 cell proliferation, spreading and alkaline phosphatase (ALP) activity than the bare MSNs, indicating good *in vitro* cytocompatibility. Simultaneously, the osteogenesis-related proteins expression and calcium mineral deposition disclose enhanced osteo-differentiation of human mesenchymal stem cells (hMSCs) under the stimulation of the p-MSNs, confirming that BFP released from MSNs could significantly promote the osteogenic differentiation of hMSCs, especially at 500 μg/mL of p-MSNs concentration. The peptide-modified MSNs with better bioactivity and osteogenic differentiation make it a potential candidate as bioactive material for bone repairing, bone regeneration, and bio-implant coating applications.

© 2015 Elsevier B.V. All rights reserved.

1. Introduction

Autogenic bone graft implantation, the current gold standard, is the major treatment modality for bone deficiencies [1], and the therapeutic success of autografts is mainly attributed to their identical chemistry and architecture to the surrounding bone tissue, as well as the presence of necessary bioactive factors required for bone regeneration [2,3]. Yet the limited availability and donor site morbidity restrict their extensive usage in the clinic. These

limitations have already led to synthetic bone grafts becoming a powerful alternative to replacing autologous grafts.

Due to the complexity of bony tissue, design and construction of synthetic bone substitution, which mimics the bone cell niche and holds great osteogenic potential, is still a challenging task for researchers. To meet the demand, various architectures of bioactive materials, such as porous metals [4,5], mesoporous materials [6,7], and nanomaterials (including nanofibrous scaffolds [8,9], nanoparticles [10–12], nanocomposites [13]), are successfully developed for bone tissue engineering, and some have achieved promising results. Specifically, mesoporous materials, with pore size in the range of 2–50 nm, including mesoporous bioactive glasses (MBGs) and mesoporous silica nanoparticles (MSNs), have attracted considerable interest for biomedical applications since mesoporous materials display favorable biocompatibility/biodegradability, and have numerous, well-defined pores that could be used to wrap the

---

* Corresponding author at: Department of Oral and Maxillofacial Surgery, School and Hospital of Stomatology, Peking University, Beijing 100081, China. Tel.: +86 1082195780.
 E-mail addresses: jiewei7860@sina.com (J. Wei), sc-wei@pku.edu.cn (S. Wei).
 [1] These authors contributed equally to this work.

Scheme 1. Schematic illustration of preparation of peptide-laden MSNs and effect of the modified MSNs on cells *in vitro*.

drug molecule inside [14,15]. Further, silicon (Si) ions released from MSNs have been shown to promote mineralized nodule formation, COL 1 synthesis, and the expression of osteogenic related genes in osteoblasts [16,17]. These advantages make MSNs promising candidates as implantable materials or drug delivery carriers for bone tissue engineering.

However, the confined bioactivity and osteogenesis ability of bare MSNs hamper their direct employment in bone regenerative medicine, which motivate researchers applying a great deal of effort to enhance the bioactivity of MSNs. For instance, increasing the specific surface area and pore volume of MSNs are reported to greatly accelerate the kinetics deposition, thus facilitating the bone-forming bioactivity of MSNs [18]. Furthermore, some groups had achieved the goals *via* introducing nutrient elements (such as calcium, magnesium), critical to human body, into MSNs to form the calcium/magnesium-doped mesoporous silica. Nevertheless, these studies are yet to imitate the natural osteogenesis microenvironment *in vivo* containing bone growth factors and cancellous inorganic minerals. Another approach is to incorporate the osteogenic protein, such as bone morphogenetic proteins (BMPs), into the mesoporous channels, and subsequently release the osteogenic proteins in a controlled/sustained fashion [19,20]. Generally, direct physical adsorption of bioactive factors onto inorganic scaffolds such as hydroxyapatite particle [21], mesoporous silica scaffold [19], and deproteinized cancellous bone [22] is a commonly utilized method, as an attempt to replicate the osteogenic niche provided by autografts.

Bone morphogenetic protein-7 (BMP-7) plays a crucial role in modulating osteogenic differentiation and proliferation, and in promoting osseointegration during new bone generation [23,24]. However, the complex multilevel structure of BMP-7 renders it prone to degradation, and tends to lose their bioactivity quickly in physiological conditions [25]. Peptides have drawn a great deal of attention currently due to their small structure and no side effect, as well as no immunogenicity compared to larger proteins [26]. Recently, Kim demonstrated that a new bone-forming peptide (BFP) sequence (GQGFSYPYKAVFSTQ) from BMP-7 had more osteogenic activity than BMP-7 and induced osteogenesis [27,28]. Therefore, the evidence of the beneficial effects of mesoporous materials as well as the osteogenic peptide factor mentioned above have motivated us to incorporate these two factors together to achieve effective local delivery of BFP for promoting the osteogenic differentiation. To the best of our knowledge, there are no previous reports in investigating the impregnation of osteogenic peptide into MSNs, and in guiding the osteogenesis of human mesenchymal stem cells (hMSCs) *in vitro*. Herein, in the present work, we first prepare and characterize the peptide-laden mesoporous silica nanoparticles (p-MSNs), and assessed the bioactivity and osteogenic commitment *in vitro* (Scheme 1).

2. Materials and methods

2.1. Synthesis and adsorption capacity of mesoporous silica

MSNs were synthesized from solutions containing a block copolymer (P123, Sigma) as the structure directing agent and tetraethyl orthosilicate (TEOS, Sigma) as a source of silica per our previous work [29,30]. To determine the required time for the system to reach equilibrium, tests were performed by immersion of 100 mg of MSNs powder into 10 mL of 10^{-4} mol/L rhodamine-labeled (TAMRA-labeled) BFP peptide (provided by Chinapeptides Co. Ltd.) in PBS (pH 7.4) in triplicate, to ensure reproducibility. The experiment was analyzed every 15 min until the system became constant, where 200 μL of supernatant was collected for calculation of the peptide remaining in solution using a fluorescence spectrophotometer (Enspire 2300-100L, PerkinElmer). The concentration of peptide was obtained by comparison with the established standard curve provided by the free labeled peptide. The adsorption capacity of MSNs with time (Q_s, adsorbate per gram of silica) was determined by the equation $Q_s = (Q_0 - Q_x)/m$, where Q_0 is the initial number of moles of the TAMRA-labeled BFP in solution, Q_x is the number of moles of TAMRA-labeled BFP remaining in solution, and m is the weight of MSNs powder.

2.2. Peptide incorporation

After determining the maximum adsorption of peptide, 100 mg of the solid material was immersed in 10 mL of 10^{-4} mol/L BFP solution (in PBS) with stirring for 30 min, as determined previously. Subsequently, the peptide-laden MSNs was washed with D.I. water thrice to remove excess non-adsorbed peptide, and dried at ambient temperature.

2.3. Characterization

The crystalline phase of the studied material was verified by X-ray diffraction (XRD, Shimadzu, Japan) with the diffraction angles between 10° and 60°. The ordered mesoporous structure of MSNs

was confirmed by small-angle X-ray diffraction (SAXRD, Rigaku, Japan) and transmission electron microscope (TEM, Tecnai F20, Philips, Netherlands). The polydispersity index (PDI) was measured by a laser particle size analyzer (Fritsch A22, Germany). Fourier transform infrared spectroscopy (FTIR, Magna-IR750, USA) and X-ray photoelectron spectroscopy (XPS, Kratos Analytical Ltd.) were employed to characterize the functional groups of the peptide-trapped MSNs. Nitrogen adsorption–desorption isotherms of samples were collected on micromeritics porosimeter (Tristar 3000, Micrometrics Instrument Corp.) at 77 K under a continuous adsorption condition.

2.4. Peptide release from p-MSNs

The release of labeled peptide from p-MSNs samples was also monitored by fluorescence spectroscopy. The TAMRA-labeled BFP laden MSNs (TB-MSNs) were first prepared. Briefly, 100 mg of MSNs powders were added into 10 mL of 10^{-4} mol/L TAMRA-labeled BFP solution for 30 min. Afterward, the TB-MSNs were separated by centrifuging, and the solid samples were dried in dark overnight at room temperature. The BFP release was evaluated by immersing TB-MSNs with the concentrations of 100 and 500 μg/mL into 10 mL of PBS buffer until the system became constant. The peptide release ratio at different time points was calculated according to the following equation: peptide mass release (%) = Q_x/Q_0, where Q_0 is the initial number of moles of the TAMRA-labeled BFP used, Q_x is the number of moles of TAMRA-labeled BFP released into the solution.

2.5. Cell culture

Human osteoblast-like MG-63 cells and hMSCs (ATCC, USA) were cultured in α-Modified Eagle's Medium (Gibco) containing 10% fetal bovine serum (Gibco), 1% (v/v) streptomycin (Amresco), and 1% (v/v) penicillin (Amresco) at 37 °C in a humidified atmosphere of 5% CO_2. The cell medium was changed every 2–3 days.

2.6. In vitro cytocompatibility of MG-63 cells

2.6.1. Assessment of internalization of MSNs

10 mg of MSNs were added to 10 mL of 0.1% (w/v) of rhodamine B isothiocyanate (Sigma) solution in dark conditions. The mixture was kept under continuous stirring, overnight, at 4 °C. Several washing steps with absolute ethanol and D.I. water were performed in order to remove the excess rhodamine. The MG-63 cells were seeded at a cell density of 1×10^4 cells/mL and allowed to adhere. After 24 h, rhodamine-labeled MSNs (0, 50, 100 and 500 μg/mL) were added to the culture wells. After another 24 h, cells were washed with PBS and fixed with 4% (w/v) paraformaldehyde in PBS for 15 min. Cell nuclei were counterstained with 10 μg/mL DAPI, and samples were visualized by a confocal laser scanning microscopy (LSM510, Carl Zeiss).
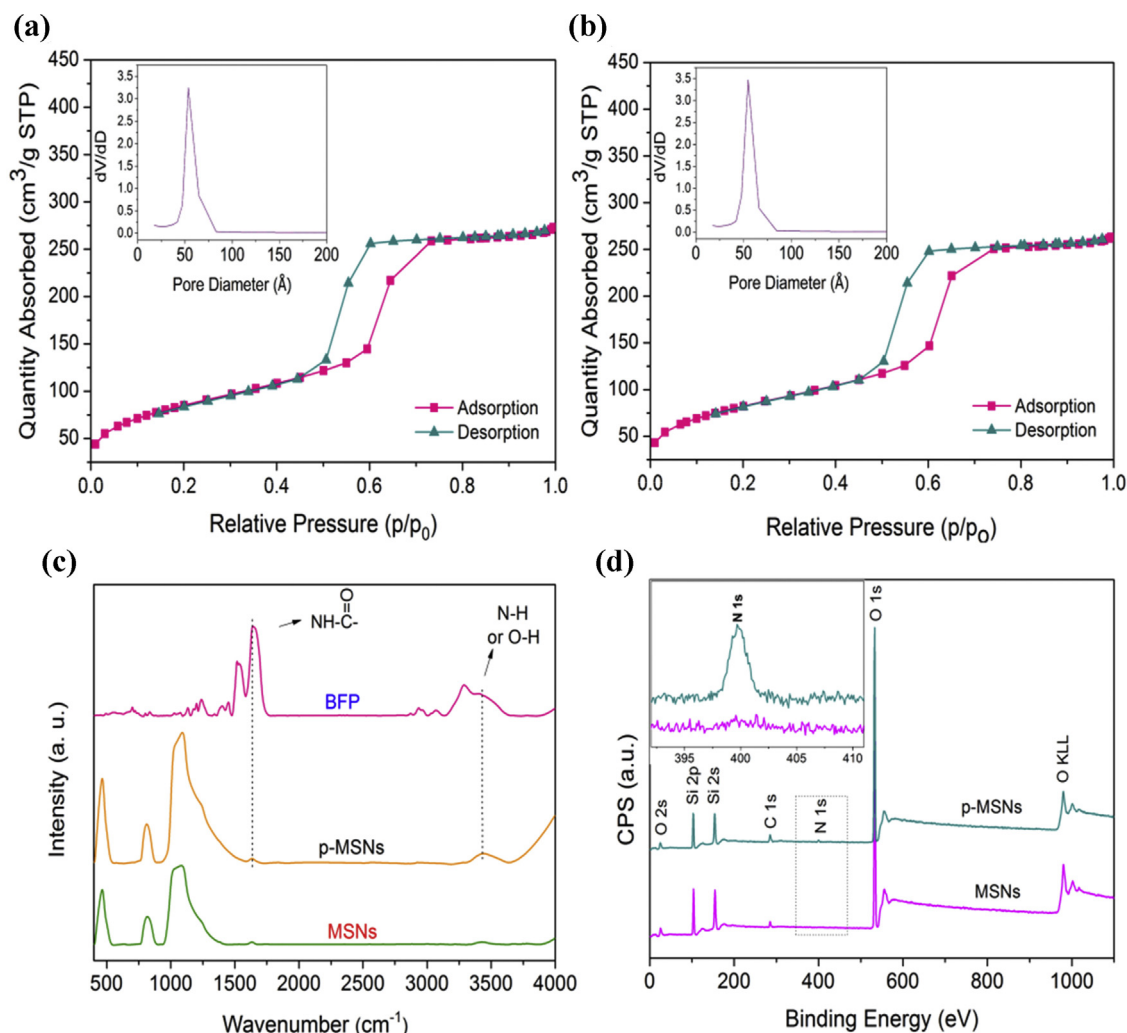

Fig. 1. Nitrogen adsorption/desorption isotherms of bare MSNs (a) and p-MSNs (b). The FT-IR spectra (c) and XPS wide spectra of (d) bare MS and p-MSNs.
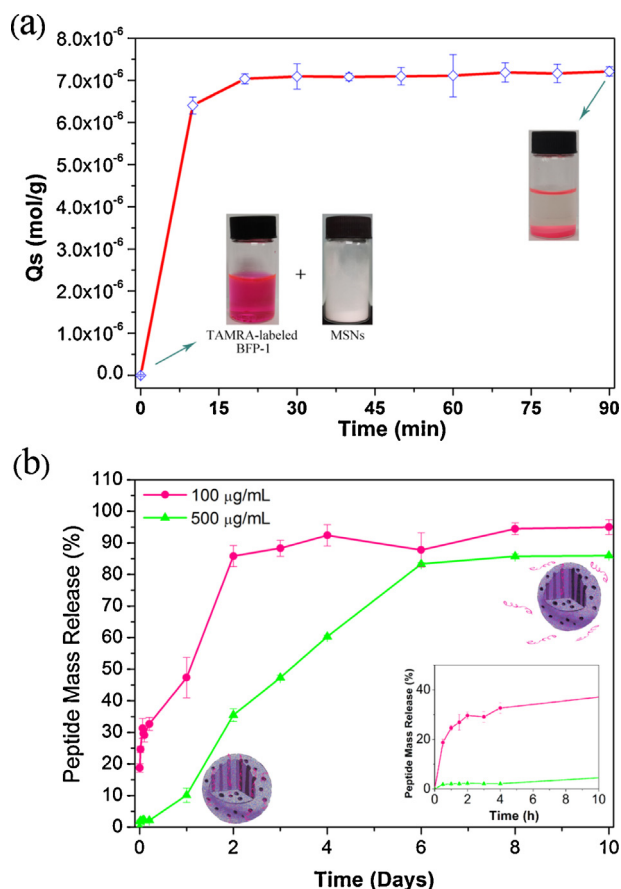
Fig. 2. (a) The maximum-time adsorption curve of BFP peptide of MSNs. (b) BFP peptide release behavior from p-MSNs; the insert highlights release at 10 h.

2.6.2. Cell viability assay

The cell counting kit-8 assay (CCK-8, Dojindo) was used to assess the viability of cells. After cell counting, MG-63 cells were seeded in 96-well plates at a density of 5×10^3 cells/well. After seeding 24 h, cells were exposed to various concentrations (5, 10, 50, 100 and 500 μg/mL) of neat MSNs and p-MSNs, respectively. The control groups involved the use of DMEM medium as negative control and 10% DMSO DMEM medium as positive control. After 1, 3 and 5 days incubation, 10 μL of CCK-8 was added into each well for 2 h incubation, and the absorbance value of supernatant optical density (OD value) was measured with a microplate reader (Model 680, Bio-Rad) at a 450 nm wavelength. The cell viability was expressed as a percentage as following:

$$Cell\ viability\ (\%)$$
$$= (OD_{(test)} - OD_{(blank)})/(OD_{(negative\ control)} - OD_{(blank)}) \times 100\%$$

2.6.3. Morphology observation of cells

MG-63 cells at 1×10^4 cells/mL were cultured on acid treated cover slips. The morphologies of MG-63 co-cultured with different concentration (100 and 500 μg/mL) of MSNs and p-MSNs were observed using a field emission scanning electron microscope (FE-SEM, S-4800, Hitachi) and metalloscope (BX51M, Olympus) after 5 days. All samples were fixed in 2.5% glutaraldehyde solution for 1 h and then dehydrated in ascending concentrations of ethanol for 15 min each. Dehydrated samples were dried by a vacuum dryer, and examined under SEM.

2.6.4. Cytoskeletal observation

After 5 days, cells at the average cell viability of about 96% were washed with PBS and fixed with 4% (w/v) paraformaldehyde for 15 min. The samples were then washed with PBS, permeabilized with 0.1% (v/v) Triton X-100 (Sigma) for 5 min, and stained with 5 μg/mL FITC-phalloidin. After washed with PBS, samples were incubated for 5 min at room temperature with 10 μg/mL DAPI. The stained signals in the cells were observed by a CLSM (LSM510, Carl Zeiss).

2.6.5. Alkaline phosphatase activity assay

Alkaline phosphatase (ALP) activity of MG-63 cells was evaluated by an assay reagent kit (Nanjing Jiancheng, China). Cells were exposed to the various concentrations of the bare MSNs and p-MSNs samples for 7 days and 14 days, respectively. The supernatant was removed and 100 μL of lysis solution (1% (v/v) TritonX-100) was added into each well and incubated for 1 h. Afterwards, 30 μL of MG-63 cell lysates at each well was transferred to new 96-well plates for ALP determination according to the manufacturer's instructions. For normalization, the total protein concentration was measured by a Bicinchoninic Acid (BCA) protein assay kit (China).

2.7. In vitro osteogenic differentiation of hMSCs

2.7.1. Ostegenic differentiation

Osteogenic inducing medium comprised fresh DMEM containing 10% FBS, 100 U/mL penicillin, 100 μg/mL streptomycin, 50 μg/mL ascorbic acid, 10 mM sodium β-glycerophosphate, and 10 nM dexamethasone L-ascorbic acid. The medium was changed every 2–3 days.

2.7.2. Immunofluorescence

After grown with different concentration of MSNs and p-MSNs for 14 days, hMSCs were fixed with 4% paraformaldehyde in PBS for 20 min, permeabilized with 0.1% Triton X-100 for 15 min and then blocked with 5% BSA in PBS for 30 min. Substrates were then incubated with primary antibodies [Rabbit Anti-Col1a1 IgG (CST) at a dilution of 1:200 and Rabbit Anti-OCN IgG (Santa, USA) at a dilution of 1:50] at 4 °C overnight, and washed with PBS twice, then incubated with secondary antibodies [Goat Anti-Rabbit Invitrogen 488 IgG, Goat Anti-Rabbit Invitrogen 647 IgG (USA)] at 1:500 for 1 h in dark. Finally, cell nuclei were stained with 10 μg/mL DAPI for 15 min. Cells were visualized immediately by the CLSM.

2.7.3. Alizarin Red Staining

Mineralized nodule formation was determined on 21 days of culture following the manufacturer's instruction through staining with Alizarin Red S (ARS) solution (Sigma). Cells layer were fixed with 4% paraformaldehyde for 30 min, and washed three times with PBS. Then a solution of 2% (w/v) ARS with pH 4.2 was added so that it covered the entire surface of the wells containing cells. After an incubation of 30 min, the excess ARS was washed with D.I. water, and the newly formed bone-like nodules on the materials were scored under the inverted phase contrast microscope (Nikon Eclipse TE2000-U).

2.8. Statistical analysis

All data were expressed as mean ± standard deviations of a representative six similar experiments carried out. Statistical analysis was performed by one-way analysis of variance (ANOVA) followed by Tukey's post hoc tests using SPSS 19.0 and p-values less than 0.05 were considered statistically significant.

3. Results and discussion

3.1. Material characterization

Fig. S1a-b presents the TEM images of the morphology of the MSNs. These images obviously show that MSNs have the particle size of about 400 nm with a PDI of 0.341, and contain cylindrical pore channels with uniform and homogeneously distributed mesoporous of the same size, which is the characteristic structure of mesoporous silica. The wide XRD pattern of MSNs is shown in Fig. S1c, where a broad diffraction peak can be seen between 15° and 35°, a typical diffraction pattern of amorphous silica, indicating that the components of MSNs are amorphous silica material. One well-resolved (1 0 0) peak and two weak signals of (1 1 0) and (2 0 0)

related with a 2D hexagonal symmetry (p6mm) are observed in SAXRD pattern of MSNs (Fig. S1d) [31,32]. These results prove that MSNs display periodic parallel channels of mesoporous materials with a hexagonal arrangement.

To further determine the average pore size and pore volume of MSNs before and after bearing peptide, the N_2 adsorption–desorption isotherm was employed. As shown in Fig. 1a, the curve exhibits that the pure MSNs have a N_2 adsorption–desorption isotherm of IV classification with a clear H1-type hysteresis loop at high relative pressure, which is characteristic of independent cylindrical slender channels with highly ordered pore size distribution [33,34], consistent with TEM observation and SAXRD analysis. The presence of hysteresis is due to incomplete filling of mesoporous, and a lower slope indicates a more homogeneous distribution
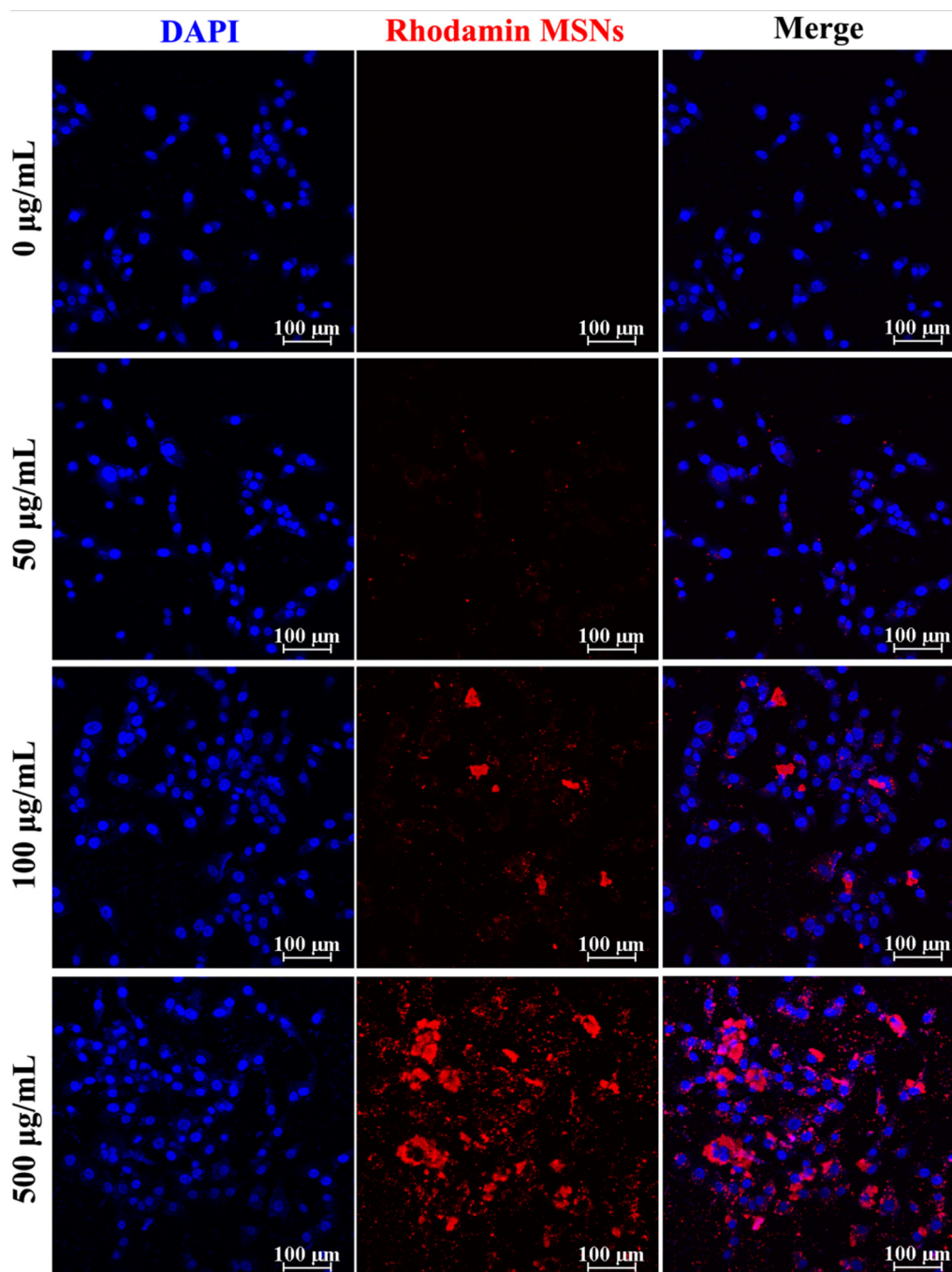

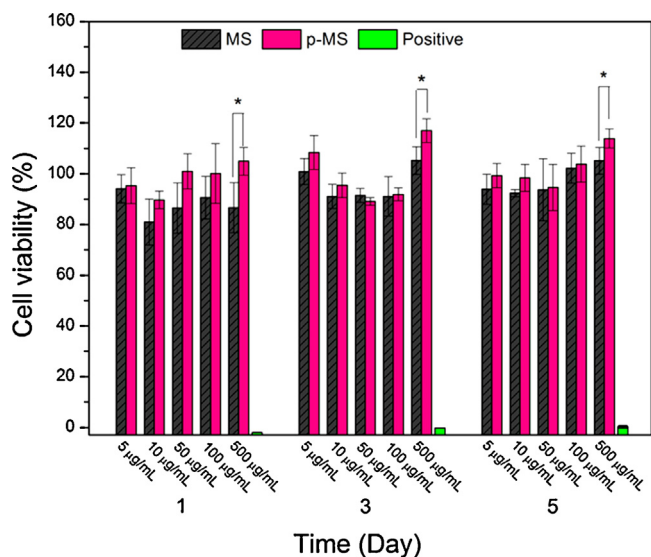
Fig. 3. The internalization of MSNs by MG-63 cells.

Fig. 4. Cell proliferation rates of MG-63 cells cultured with different concentrations of pristine MSNs and peptide-laden MSNs, * $p < 0.05$.

of pore sizes. No significant difference can be detected between adsorption–desorption isotherms for the bare MSNs (Fig. 1a) and p-MSNs samples (Fig. 1b). Furthermore, Table S1 shows that based on the calculation by the BET and BJH method, there is only a slight reduction in the average pore size from 5.56 to 4.95 nm, specific surface area from 304.09 to 292.41 m^2/g and pore volume from 0.44 to 0.42 cm^3/g after peptide entrapment, which confirms that the peptide decoration has no influence on mesoporous structure of the MSNs. The remaining mesoporous could provide an extra room to load another bioactive molecules (natural proteins or mucopolysaccharides) for endowing mesoporous materials more excellent biological performances.

Fig. 1c compares the FTIR spectra of the neat MSNs and p-MSNs. In both samples, the typical broad peaks, attributed to symmetric stretching of OH groups, ν_s (HOH) and ν_s (SiO—H), at 3445 cm^{-1} and a weak peak, due to the deformation of OH groups, δ(HOH), at 1638 cm^{-1} are observed. Furthermore, the spectra show the main characteristic peaks of silica in the region around 1091 cm^{-1} corresponding to ν_{as}(Si—O—Si), 813 cm^{-1} associated with ν_s(Si—O—Si) and δ(O—Si—O) deformation at 460 cm^{-1}. However, after the decoration of peptide, the intensity of peaks is enhanced at about 1640 cm^{-1} and 3445 cm^{-1} which might result from the superimposed vibration of amide groups (NH—C=O)/OH groups and δ(N—H)/OH groups, respectively, because the BFP peptide displays two strong characteristic peaks of amide groups at 1645 cm^{-1} and δ(N—H) at 3459 cm^{-1}, illustrating that the peptide is loaded into the mesoporous of MSNs successfully. To verify the results obtained from the FT-IR analysis, XPS is applied to evaluate the detail chemical bonds and elements of the bare MSNs and peptide-laden MSNs. As shown in Fig. 1d, the pristine MSNs exhibit silicon and oxygen peaks as the main atomic elements, whereas a new and obvious nitrogen peak appears in the XPS spectrum for the peptide-laden MSNs sample. The appearance of nitrogen signal (N 1s), which is the characteristic element of peptide, in the high resolution narrow spectrum and its enhanced intensity in the peptide-encapsulated MSNs, further indicate the successful incorporation of BFP. Furthermore, an evident change in carbon bond composition observed in the high-resolution narrow carbon spectra (C 1s) clearly supports these conclusions (Fig. S2). The high-resolution C 1s spectra of the bare MSNs are deconvoluted into three different curves. The binding energies centered at 284.8 eV, 286.5 eV and 289.0 eV are assigned to the carbon skeleton (C—C/C—H), hydroxyl group

(C—OH), carbonyl group (C=O), respectively [35,36]. Nevertheless, a broad peak assigned to the —C—N— bond at about 285.5 eV is recorded on the p-MSNs samples, indicating the presence of peptide. In addition, after peptide immobilization, the intensity of the carbon skeleton (—C—C—/—C—H—) peak decreases dramatically, and the peaks of the hydroxyl (C—OH) and carbonyl groups (C=O) increase as shown in Fig. S2b. They should be attributed to the carboxyl groups (COOH) and amide bond groups (—NH—C=O) in the structure of BFP peptide molecule.

3.2. The adsorption and release behavior of p-MSNs

In order to determine the maximum-time for the system to reach equilibrium and adsorption capacity, the adsorption curve is plotted to calculate the amount of the peptide adsorbed into the MSNs in PBS. Fig. 2a shows that the red TAMRA-labeled BFP is adsorbed by the mesoporous of the samples when MSNs are added, resulting in the disappearance of red color, and the white MSNs powders turn into red sediments at the bottom after 25 min, from which the excellent capacity of MSNs for adsorption could be seen visually. The analysis of the graph shows that the MSNs powders reach equilibrium in approximately 25 min, and they have a maximum adsorption capacity at 7.1×10^{-6} mol/g, corresponding to about 72% of the moles of BFP present in the starting solutions. Such excellent adsorption capacity is probably contributed to the high specific surface area (304.09 m^2/g) of MSNs and the high affinity of the negative surface of silica with the peptide and the positive charge at pH 7.4. It is known that biomolecules and polymers containing positively charged residues have high affinity for silica surfaces that display a negative surface charge at neutral pH due to the presence of deprotonated hydroxyl groups on the surface [37,38]. Hence, the favorable incorporation of BFP peptide may be due to the hydrogen bonding or long-range electrostatic ionic amine bonds (Si—O$^-$—$^+$H$_3$N) formed between the silanol group present in the MSNs and the N-terminal side chains of the Gln, Thr amino acids or the amino group of the first Ala amino acid.

The cumulative release profiles *versus* time are shown in Fig. 2b for the peptide-laden MSNs at 100 and 500 µg/mL, respectively. It can be seen that a large amount of adsorbed peptide is released, suggesting outstanding release behavior. However, the difference in the amount of BFP released of the two curves is observed, suggesting that the release capacity could be independent of the concentration of MSNs powder. Peptide molecules are almost completely released from the MSNs at 100 µg/mL in the first 2 days, with a fast rate of delivery for up to 10 h. However, for the concentration at 500 µg/mL, the p-MSNs present more sustained drug release patterns. An initial burst release of peptide is observed during the first 2 days, which accounts for around 37% of the total loaded peptide. Subsequently, another 46% dose of peptide is released in a comparatively sustained manner and lasted for more than 6 days. The reason could be attributed to that in the high concentration of p-MSNs system there is a larger amount of peptide released from MSNs into solution, resulting in the reduction of the density gradient that is the impetus of delivery.

3.3. In vitro cytotoxicity evaluation

The cytotoxicity of the as-prepared peptide-laden MSNs to human osteoblast-like MG-63 cells is another critical factor that should be carefully evaluated when the novel peptide-encapsulated MSNs is used in biomedical applications. Previous reports demonstrate that MSNs crystals could be toxic to cells in a concentration-dependent manner through the cellular uptake [39,40]. As shown in Fig. 3, the internalization of silicate nanoparticles can be confirmed by CLSM observation. The addition of up to 50 µg/mL MSNs to the cells does not cause the significant

internalization of cells. However, at concentrations ranging from 100 to 500 μg/mL, labeled MSNs get internalized and widely distributed in the cell cytoplasm around the cells nuclei, and at higher concentration of MSNs, more cells interacted with the MSNs. Next, we test the potential cytotoxicity of the peptide-laden MSNs, and Fig. 4 shows the MG-63 cells co-cultured with different concentrations (5, 10, 50, 100, and 500 μg/mL) of the bare MSNs and BFP-laden MSNs powders in DMEM for 1, 3 and 5 days, respectively. We observe that the pristine MSNs and p-MSNs do not show toxicity up to a reasonably high concentration of 500 μg/mL, suggesting that p-MSNs are nontoxic and biocompatible for use as a growth factor delivery system. The cells cultured with the pure MSNs and peptide-laden MSNs show no statistical difference in cell viability below the concentration of 100 μg/mL, in the case of high MSNs content, however, cells cultured with 500 μg/mL of p-MSNs have superior cell viability than those of pristine MSNs and display higher than 100% cell viability at each time point. The peptide content released from peptide-decorated MSNs can affect the *in vitro* cytocompatibility of the samples, and 500 μg/mL of p-MSNs could facilitate the proliferation of MG-63 cells. Meanwhile, based on our

results 500 μg/mL may be the minimal concentration of the p-MSNs for steering the cellular fate.

3.4. Cellular morphology and cytoskeletal observation

To further examine the toxicity of p-MSNs powders, adherent morphologies of the MG-63 cells are examined. The typical overview of MG-63 cells morphologies growing with different concentrations (100 and 500 μg/mL) of bare MSNs and p-MSNs powders for 5 days is shown in Fig. 5. From the enlarged images, it can be seen that MG-63 cultured on all the samples show a healthy shape. Compared with that of bare MSNs counterpart, higher amount of cells with better adhesion and spreading is observed in the peptide-laden MSNs group. In addition, it could be seen that MG-63 cells exhibit extended morphology with many pseudopodium and a cytoplastic shape on the surface of p-MSNs, which is also demonstrated by the metalloscope observation of MG-63 cells (Fig. S3). The fluorescence images from Fig. 5b indicate that MG-63 cells show limited spreading and display filamentous morphology on the pristine MSNs powders regardless of 100 or
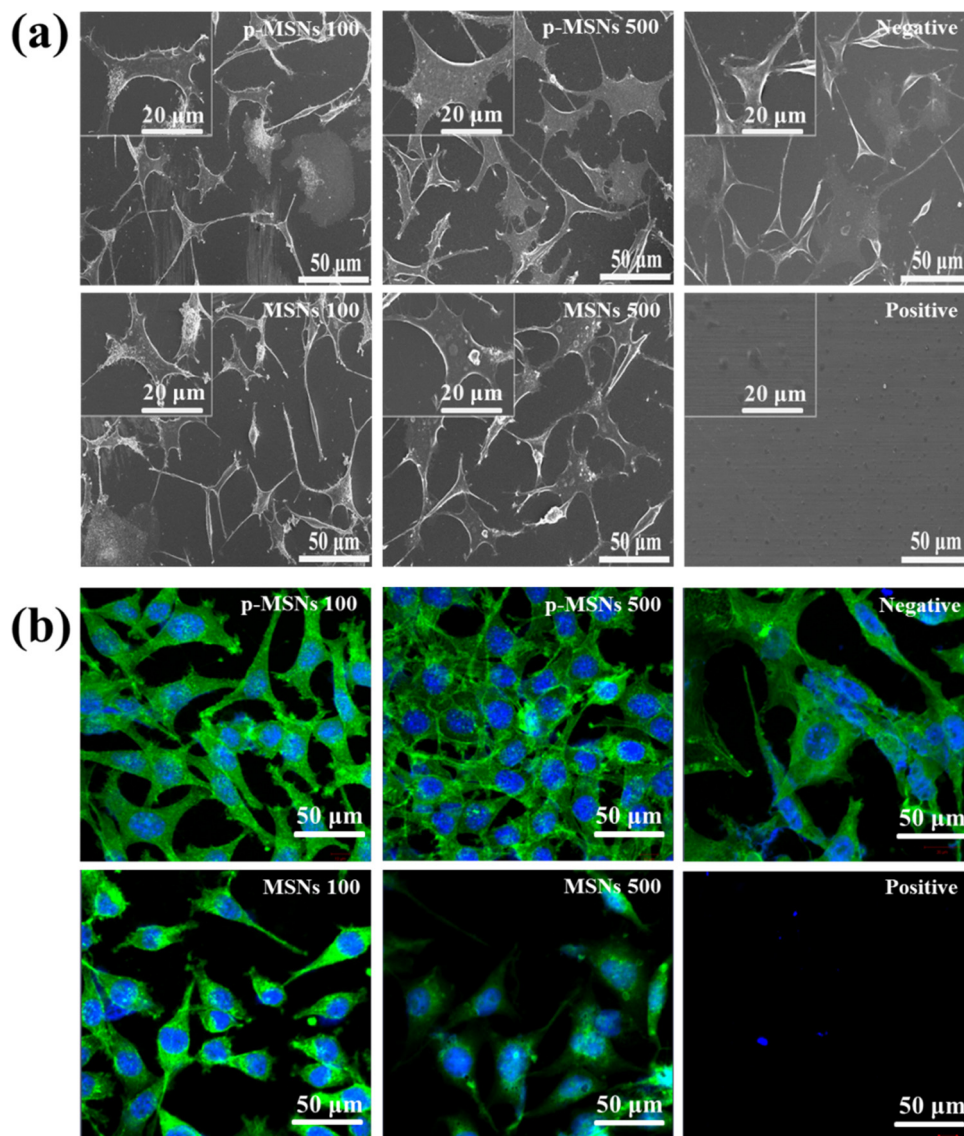

Fig. 5. (a) SEM images of MG-63 cells; (b) adhesion morphology and actin cytoskeletal organization (green, labeled with FITC-phalloidin, counterstained with DAPI for nuclei in blue) of MG-63 after incubation with pristine MSNs and p-MSNs. Average cell viability at about 96%. (For interpretation of the references to colour in this figure legend, the reader is referred to the web version of this article.)
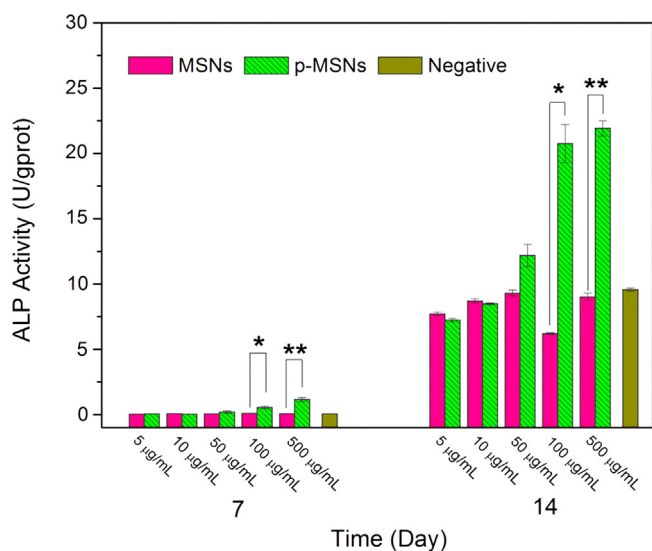
Fig. 6. ALP activity of MG-63 after cultivating for 7 and 14 days, respectively, with the pristine MSNs and peptide-laden MSNs of different concentrations. * $p < 0.05$, **$p < 0.01$.

500 µg/mL, and F-actin is poorly developed. However, in p-MSNs group, MG-63 cells attach and spread more than the pristine MSNs group, indicating that the released peptide has enhanced cell adhesion. In comparison to the pristine MSNs at 100 and 500 µg/mL and p-MSNs at 100 µg/mL, much more MG-63 cells adhere onto 500 µg/mL of p-MSNs sample. Furthermore, with enhanced cell adhesion, MG-63 cells cultured with p-MSNs group extend more adhered filopodia and spread more with visible presentation of more mature F-actin intracellular stress fibers, suggesting that p-MSNs have good *in vitro* cytocompatibility. These cell observation results could be attributed to the different peptide content delivered from the p-MSNs. We calculate the amount of BFP released form p-MSNs from the adsorption curve and release curve in Fig. 2. Approximately 0.61 µg/mL peptide and 0.67 µg/mL peptide are delivered from p-MSNs at the 1st day from p-MSNs at 100 and 500 µg/mL in 24-well plates, respectively. Nevertheless, 500 µg/mL p-MSNs release about three-fold of peptide concentration (3.35 µg/mL) than that of 100 µg/mL p-MSNs (1.17 µg/mL) at the 3rd day, which leads to better cell behaviors (cell proliferation, spreading and morphology).
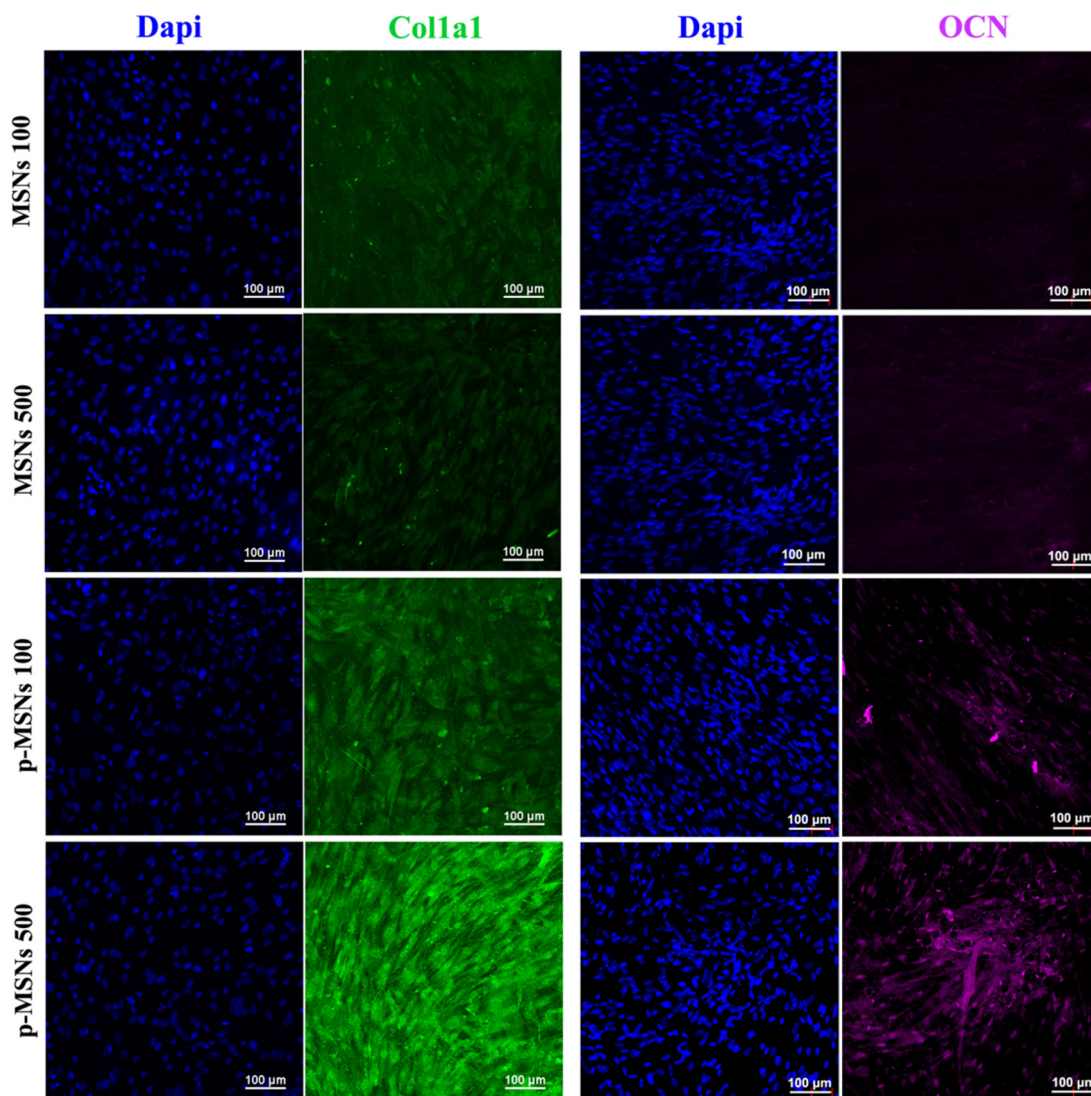

Fig. 7. Immunofluorescence staining for osteogenesis-related proteins including Col1a1 (green), and OCN (pink) at 14 days. Nuclei were stained blue with DAPI. (For interpretation of the references to colour in this figure legend, the reader is referred to the web version of this article.)

3.5. Alkaline phosphatase activity (ALP)

To successfully apply peptide-laden MSNs technology in bone repairing engineering, high osteogenic differentiation activity is pivotal, therefore, the osteoblastic phenotypic expression of the BFP laden p-MSNs is necessary to be examined. Alkaline phosphate (ALP) is an important indication of osteoblast cells expressed in their differentiation phase and a significant quantitative marker of osteogenesis at 7–14 days [41,42]. As depicted in Fig. 6, ALP activities increase with time when MG-63 cells are co-cultured with different MSNs, indicating that nanosized mesoporous silica could induce the osteogenic differentiation of cells. However, much higher ALP expression is detected in the case of the peptide-laden MSNs at 7 and 14 days, which suggests that the functionalization of the mesoporous silica with BFP could further enhance the mineralization and cell activation of MG-63 cells. The dose-dependent osteogenic activity is also found for MG-63 cell cultured with different concentrations of the pristine MSNs and p-MSNs groups. No significant difference is found for the ALP production in various concentrations of the pristine MSNs at 7 and 14 days. Nevertheless, there is a clear positive concentration-dependence property for the peptide-laden MSNs. As for p-MSNs, the ALP expression elevates as the increasing of nanopartiles density, which is significantly different from that of the pristine MSNs. Obviously, ALP activities of MG-63 cells cultured with p-MSNs at 100 and 500 μg/mL exhibit statistical difference to bare MSNs groups after 7 days and 14 days. These suggest that when the concentration of p-MSNs is up to 100 μg/mL, p-MSNs release sufficient BFP molecule to trigger the osteogenic path of bone cells. In addition, p-MSNs at 500 μg/mL display greatest osteogenic differentiation activity, consistent with the CCK-8 assay results in Fig. 4.

3.6. Immunofluorescence and matrix mineralization

The osteogenic potential of peptide-laden MSNs is further proved by culturing hMSCs, a type of non-differentiated cells, through immunofluorescence staining and calcium deposition. As shown in Fig. 7, the bare MSNs present the lowest expression of osteo-related proteins, indicating the defective osteogenesis ability. However, higher density of Col1a1 (green, one of the major components in the extracellular matrix and accounts for 90% of the protein mass in the organic part of bone) and OCN (red, a calcium binding protein, marker for the bone formation process and playing an important role in bone-building) are shown in the peptide-trapped MSNs groups, owning to the increased cell proliferation and ALP activity in the presence of BFP peptide. Between these two peptide-laden MSNs, the Col1a1 and OCN expression in p-MSNs at 500 μg/mL are much stronger than that at 100 μg/mL. This is because more peptide content releases from MSNs at 500 μg/mL, in accordance with ALP results of MG-63 cells.

The production of calcium deposit at the late stage of differentiation is another critical indicator for osteogenic efficiency of hMSCs. ARS stain which specifically binds to highly enriched calcium deposits is generally employed to confirm the presence of mineralized cells. As the osteogenic culture of hMSCs under different MSNs progress to 21 days, cells start to aggregate together and form bone-like structures which are stained for ARS. The hMSCs cultured in bare MSNs at both 100 and 500 μg/mL form small numbers of bone nodules in osteogenic inducing medium as seen in Fig. S4. After combination with BFP-1 peptide, however, the osteogenic efficiency is greatly enhanced, which is reflected by the greater amounts and larger size of bone nodules compared with the pure MSNs groups. Similar to the trend observed with immunofluorescence, more intensively distributed and bigger bone nodules are observed in p-MSNs at 500 μg/mL. As mentioned above, BFP peptide derived from the immature region of BMP-7 protein holds the

similar osteogenic inducing property, and may bind to the same functional sites (BMP receptors), triggering the up-regulation of target osteogenic genes through Smads or mitogen-activated protein kinase (MAPK) [43], therefore facilitating bone formation.

4. Conclusion

In summary, we have successfully synthesized MSNs with ordered mesoporous structure, and incorporated BFP into the silica-based mesoporous materials to obtain peptide-laden MSNs for enhanced osteogenic differentiation. FT-IR and XPS confirm that the peptide is successfully laden into the mesoporous of MSNs. The adsorption curves suggest that MSNs have outstanding loading capacity, additionally, the p-MSNs at 500 μg/mL show more sustained peptide release rate and could provide sufficient peptide concentrations over 6 days in vitro. After 5 days incubation, the peptide-trapped MSNs exert a positive effect on in vitro cell proliferation and spreading toward MG-63 cells, especially at the concentration of 500 μg/mL, which reveal that p-MSNs exhibit excellent biocompatibility. Moreover, the peptide-functionalization of MSNs could further elevate the osteogenesis-related proteins expression and bone matrix mineralization of hMSCs, proving that the biological activity of the peptide released from MSNs could be maintained and BFP could significantly promote the osteogenic differentiation of hMSCs. The present study could broaden the application of MSNs as biocomposite and provide new prospects for utilizing the peptide-laden MSNs in bone repair substitutes.

Appendix A. Supplementary data

Supplementary data associated with this article can be found, in the online version, at http://dx.doi.org/10.1016/j.colsurfb.2015.04.043

References

[1] R.R. Betz, Orthopedics 25 (2002) s561.
[2] C. Perka, O. Schultz, R.S. Spitzer, et al., Biomaterials 21 (2000) 1145.
[3] X. Zhang, M. Xu, L. Song, et al., Biomaterials 34 (2013) 9103.
[4] S. Fujibayashi, M. Neo, H.M. Kim, et al., Biomaterials 25 (2004) 443.
[5] S.A. Yavari, J. van der Stok, Y.C. Chai, et al., Biomaterials 35 (2014) 6172.
[6] Y. Zhu, C. Wu, Y. Ramaswamy, et al., Microporous Mesoporous Mater. 112 (2008) 494.
[7] C. Wu, Y. Zhou, W. Fan, et al., Biomaterials 33 (2012) 2076.
[8] F. Ding, H. Deng, Y. Du, et al., Nanoscale 6 (2014) 9477.
[9] H. Peng, X. Liu, R. Wang, et al., J. Mater. Chem. B: Mater. Biol. Med. 2 (2014) 6435.
[10] Q. Wang, Z. Gu, S. Jamal, et al., Tissue Eng. A 19 (2013) 2586.
[11] Q. Wang, J. Wang, Q. Lu, et al., Biomaterials 31 (2010) 4980.
[12] Q. Wang, L. Wang, M.S. Detamore, et al., Adv. Mater. 20 (2008) 236.
[13] F. Song, X. Li, Q. Wang, et al., J. Biomed. Nanotechnol. 11 (2015) 40.
[14] N. Singh, A. Karambelkar, L. Gu, et al., J. Am. Chem. Soc. 133 (2011) 19582.
[15] Z. Chen, X. Li, H. He, et al., Colloids Surf. B: Biointerfaces 95 (2012) 274.
[16] P. Han, C. Wu, Y. Xiao, Biomater. Sci. 1 (2013) 379.
[17] J. Sun, L. Wei, X. Liu, et al., Acta Biomater. 5 (2009) 1284.
[18] Y.C. Kuo, C.C. Wang, Colloids Surf. B: Biointerfaces 84 (2011) 63.
[19] T.H. Kim, M. Kim, M. Eltohamy, et al., J. Biomed. Mater. Res. A 101 (2013) 1651.
[20] Q. Gan, J. Zhu, Y. Yuan, et al., J. Mater. Chem. B (2014).
[21] T. Matsumoto, M. Okazaki, M. Inoue, et al., Biomaterials 25 (2004) 3807.
[22] T. Liu, G. Wu, D. Wismeijer, et al., Bone 56 (2013) 110.
[23] L. Zhi, C. Chen, X. Pang, et al., Int. Orthop. 35 (2011) 1889.
[24] R.S. Carpenter, L.R. Goodrich, D.D. Frisbie, et al., J. Orthop. Res. 28 (2010) 1330.
[25] J. Lock, H. Liu, Int. J. Nanomed. 6 (2011) 2769.
[26] L. Mendes, S. Saska, M. Martines, et al., Mater. Sci. Eng. C: Mater. Biol. Appl. 33 (2013) 4427.
[27] H.K. Kim, J.H. Kim, D.S. Park, et al., Biomaterials 33 (2012) 7057.
[28] Y.J. Lee, J.H. Lee, H.J. Cho, et al., Biomaterials 34 (2013) 5059.

[29] Z. Wu, T. Tang, H. Guo, et al., Colloids Surf. B: Biointerfaces 120 (2014) 38.
[30] C. Dai, H. Guo, J. Lu, et al., Biomaterials 32 (2011) 8506.
[31] D. Zhao, J. Feng, Q. Huo, et al., Science 279 (1998) 548.
[32] C. Dai, C. Liu, J. Wei, et al., Biomaterials 31 (2010) 7620.
[33] E.P. Barrett, L.G. Joyner, P.P. Halenda, et al., J. Am. Chem. Soc. 73 (1951) 373.
[34] I. Izquierdo-Barba, E. Sousa, J.C. Doadrio, et al., J. Solgel Sci. Technol. 50 (2009) 421.
[35] Y. Deng, X. Zhang, X. Zhao, et al., Acta Biomater. 9 (2013) 8840.
[36] C. Cheng, S. Nie, S. Li, et al., J. Mater. Chem. B: Mater. Biol. Med. 1 (2013) 265.
[37] E. Eteshola, L.J. Brillson, S.C. Lee, et al., Biomol. Eng. 22 (2005) 201.
[38] V. Puddu, C.C. Perry, ACS Nano 6 (2012) 6356.
[39] X. Huang, X. Teng, D. Chen, et al., Biomaterials 31 (2010) 438.
[40] J.L. Vivero-Escoto, I.I. Slowing, V.S.Y. Lin, Biomaterials 31 (2010) 1325.
[41] S. Hattar, A. Berdal, A. Asselin, et al., Eur. Cell Mater. 4 (2002) 61.
[42] Q. Li, M. Li, P. Zhu, et al., J. Mater. Chem. 22 (2012) 20257.
[43] H. Senta, H. Park, E. Bergeron, et al., Cytokine Growth Factor Rev. 20 (2009) 213.